arXiv:1607.07338v2 [cond-mat.quant-gas] 25 Oct 2016

Nanoscale 'Dark State' Optical Potentials for Cold Atoms

M. Łącki,[1,2] M. A. Baranov,[1,2] H. Pichler,[1,2,3,4] and P. Zoller[1,2]

[1] *Institute for Quantum Optics and Quantum Information of the Austrian Academy of Sciences, A-6020 Innsbruck, Austria*
[2] *Institute for Theoretical Physics, University of Innsbruck, A-6020 Innsbruck, Austria*
[3] *ITAMP, Harvard-Smithsonian Center for Astrophysics, 60 Garden Street, Cambridge, MA 02138, USA*
[4] *Physics Department, Harvard University, 17 Oxford Street, Cambridge, Massachusetts 02138, USA*

(Dated: October 26, 2016)

We discuss generation of subwavelength optical barriers on the scale of tens of nanometers, as conservative optical potentials for cold atoms. These arise from nonadiabatic corrections to Born-Oppenheimer potentials from dressed 'dark states' in atomic Λ-configurations. We illustrate the concepts with a double layer potential for atoms obtained from inserting an optical subwavelength barrier into a well generated by an off-resonant optical lattice, and discuss bound states of pairs of atoms interacting via magnetic dipolar interactions. The subwavelength optical barriers represent an optical 'Kronig-Penney' potential. We present a detailed study of the bandstructure in optical 'Kronig-Penney' potentials, including decoherence from spontaneous emission and atom loss to open 'bright' channels.

PACS numbers: 37.10.Jk,32.80.Qk,37.10.Vz

Optical potentials generated by laser light are a fundamental tool to manipulate the motion of cold atoms with both conservative and dissipative forces [1, 2]. Paradigmatic examples of conservative optical potentials are optical dipole traps from a focused far off-resonant light beam, or optical lattices (OL) generated by an off-resonant standing laser wave, as basis of the ongoing experimental effort to realize atomic Hubbard models [2]. The underlying physical mechanism is the second-order AC Stark shift of an electronic atomic level, which is proportional to the light intensity. Optical potential landscapes, which can be designed, will thus reflect, and be limited by the achievable spatial variation of the light intensity. For light in the far-field, i.e. for optical trapping far away from surfaces (compare [4–8]), this spatial resolution will thus be given essentially by the wavelength of the light λ. In the quest to realize free-space optical subwavelength structures for atoms [9–15] we will describe and study below a family of conservative optical potentials, which arise as *nonadiabatic corrections to dark states* (DSs) in atomic Λ-type configurations [16, 17], building on the strong nonlinear atomic response to the driving lasers. The present scheme should allow the realization of *optical barriers* for atoms on the scale of tens of nanometers, and in combination with traditional optical potentials and lattices the formation of a complex 'nanoscale' optical landscape for atoms. Our discussion should be of particular interest for realizing many-atom quantum dynamics as a strongly interacting many-body systems, where atomic energy scales and interactions, such as magnetic dipolar couplings [18–22], are strongly enhanced by subwavelength distances.

To illustrate the 'nanoscale' optical potentials we can construct, we show in Fig. 1 a setup, where a subwavelength barrier of width ℓ is inserted into a potential well. This potential well can be created, for example, with a (standard) off-resonant OL $V_L(x) = V_0 \sin^2(k_L x) \approx V_0 (k_L x)^2$ with $\lambda_L \equiv 2\pi/k_L$ the wavelength of the trapping laser, and we denote its ground state size by a_L. Thus our aim is to create a double well potential for atoms on the subwavelength scale $\ell \ll a_L \ll \lambda_L/2$. By adjusting the height, and by displacing the subwavelength barrier we can control the tunnel coupling between the wells, strongly enhanced relative to the standard OL with lattice period $\lambda_L/2$. In a 3D (2D) setup this realizes a *double layer (wire), with subwavelength separation.* Loading magnetic atoms or polar molecules with dipolar interactions into these structures we benefit from the strongly enhanced energy scales for interlayer(wire) interactions.

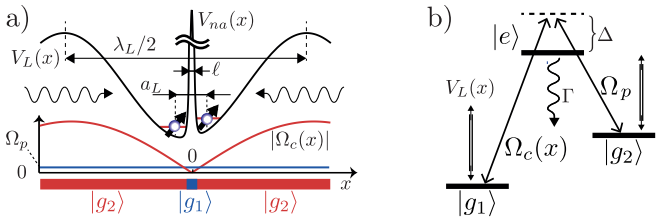

FIG. 1. (Color online) (a) A double well potential for atoms is created by inserting an optical subwavelength barrier $V_{na}(x)$ with width ℓ into a potential well generated with an off-resonant OL $V_L(x)$ with lattice period $\lambda_L/2$, and size of the vibrational ground state a_L, such that $\ell \ll a_L \ll \lambda_L/2$. The subwavelength barrier is obtained with an atomic Λ-system supporting a 'dark state' as superposition of the two atomic ground states $|g_1\rangle$ and $|g_2\rangle$ (b), where a resonant Raman coupling from a strong control field $\Omega_c(x) = \Omega_c \sin(kx)$ ($k = 2\pi/\lambda$) and a weak probe field Ω_p connects the two ground states (see text).

We propose and analyze below the physical realization of such a setup, and we will mainly focus on a 1D model considering atomic motion along x. The subwavelength barrier is obtained by choosing an atomic Λ-transition with two long-lived ground (spin) states $|g_1\rangle \equiv |\downarrow\rangle$, $|g_2\rangle \equiv |\uparrow\rangle$ (Fig. 1b) [23, 24], which are coupled by a Raman tran-

sition. The first leg of the Raman coupling is a strong control laser with Rabi frequency $\Omega_c(x) = \Omega_c \sin(kx)$ as a standing wave with wavelength $\lambda = 2\pi/k$ along x, and the second is a weak probe laser with Rabi frequency Ω_p with propagation direction perpendicular to the axis x [25]. We denote the ratio of Rabi frequencies as $\epsilon \equiv \Omega_p/\Omega_c \ll 1$. The lasers are tuned to satisfy the Raman resonance condition, while the detuning Δ from the excited state $|e\rangle$ can be near or off-resonant. The relevant Hamiltonian is $H = -\hbar^2\partial_x^2/2m + H_a(x)$ [23], as a sum of the kinetic energy and the internal atomic Hamiltonian

$$H_a = \hbar\left[\left(-\Delta - i\frac{\Gamma}{2}\right)|e\rangle\langle e| + \frac{\Omega_c(x)}{2}|e\rangle\langle g_1| + \frac{\Omega_p}{2}|e\rangle\langle g_2| + \text{h.c.}\right]$$

written in a rotating frame and with Γ the spontaneous decay rate of $|e\rangle$. We can add to the above Hamiltonian a trapping potential for the ground states $V(x)$ to generate the well of Fig. 1. This is realized, e.g. as a 1D off-resonant lattice $V_L(x) = V_0 \sin^2(k_L x)$ with an effective $k_L = 2\pi/\lambda_L$, i.e. $V(x) \equiv V_L(x)\sum_{i=1,2}|g_i\rangle\langle g_i|$. This far off-resonant OL potential acts equally on both ground states, and thus preserves the resonance Raman condition independent of x.

We are interested in the regime of slow atomic motion, where the kinetic energy (and trapping potential $V(x)$) are small relative to the energy scales set by H_a. In the spirit of the Born-Oppenheimer (BO) approximation [26–29] we diagonalize $H_a(x)|E_\sigma(x)\rangle = E_\sigma(x)|E_\sigma(x)\rangle$ ($\sigma = 0, \pm$) to obtain position dependent dressed energies,

$$E_0(x) = 0, \quad E_\pm(x) = \frac{\hbar}{2}\left[-\tilde{\Delta} \pm \sqrt{\Omega_p^2 + \Omega_c^2(x) + \tilde{\Delta}^2}\right]$$

with $\tilde{\Delta} \equiv \Delta + i\frac{\Gamma}{2}$, playing the role of adiabatic BO potentials for the atomic motion. Such a Λ-configuration supports an atomic DS $E_0 = 0$ as a linear combination of the ground states, $|E_0(x)\rangle = -\cos\alpha(x)|g_1\rangle + \sin\alpha(x)|g_2\rangle$ with $\alpha(x) = \arctan[\Omega_c(x)/\Omega_p]$, which for an atom at a given position x (at rest) is decoupled from the exciting Raman beams. The identity of this DS changes in space on a subwavelength scale [10, 24]: in regions $|\Omega_c(x)| \gg \Omega_p$ we have $|E_0\rangle \sim |g_2\rangle$, while $|\Omega_c(x)| \ll \Omega_p$ defines a region $\ell \equiv \epsilon\lambda/2\pi \ll \lambda$ with $|E_0\rangle \sim |g_1\rangle$ and thus a spatial *subwavelength spin structure* (bottom of Fig. 1a).

An atom prepared in the DS, and moving slowly in space will, in accordance with an adiabaticity requirement [30], remain in this DS, and the internal state will change its internal spin identity according to $|E_0(x)\rangle$ on the scale $\ell \ll \lambda$. Correspondingly, there will be nonadiabatic corrections to this motion. As shown below, these nonadiabatic corrections take on the form of a *subwavelength optical barrier* representing a *conservative potential*

$$V_{na}(x) = \frac{\hbar^2}{2m}(\partial_x\alpha)^2 \equiv E_R\frac{\epsilon^2\cos^2(kx)}{[\epsilon^2 + \sin^2(kx)]^2} \qquad (1)$$

with $E_R = \hbar^2k^2/2m$ the recoil energy and atomic mass m. The effective 1D Hamiltonian for the atomic motion

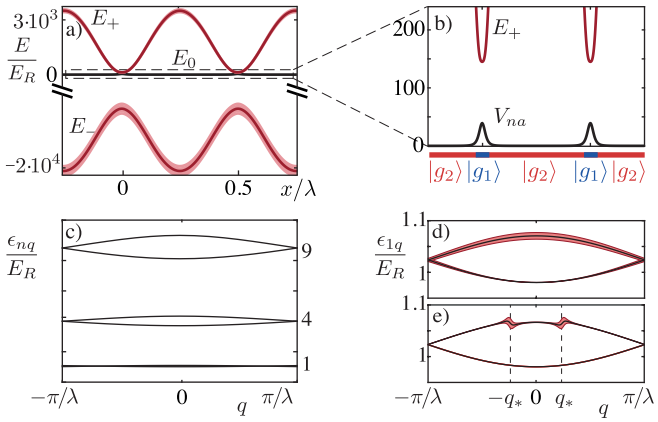

FIG. 2. (Color online) a) BO potentials $E_0(x) = 0$ (black line) and $E_\pm(x)$ (red line, with line width indicating Im $E_\pm(x)$) for DS and BS, respectively. Parameters: $\Omega_c = \Delta = 1.7\times10^4 E_R$, $\epsilon = 0.16$, $\Gamma = 5\times10^2 E_R$. b) Zoom showing $V_{na}(x)$ (black) and the lower part of $E_+(x)$ (red). c) Lowest Bloch bands $\epsilon_{n,q}$ for $V_{na}(x)$ for Brillouin zone $|q| < \pi/\lambda$ (see text); $\epsilon = 0.1$. d), e) Zooms of the lowest Bloch band of the DS lattice, including couplings to BSs for $\epsilon = 0.1, \Omega_p = 2\times10^3 E_R$, $\Gamma = 10^3 E_R$ (d), and $\Gamma = 10E_R$ (e) (see text and [32]). Black lines indicate Re $\epsilon_{1,q}$, and red shadings the widths Im $\epsilon_{1,q} = -\hbar\gamma_{1,q}/2$.

is thus $h = -\hbar^2\partial_x^2/2m + V_L(x) + V_{na}(x)$. In Fig. 1a this realizes the subwavelength barrier, where the vibrational ground state of the OL potential $V_L(x)$ of size a_L is split into a double well for $\ell \ll a_L$. We note that $V_{na}(x)$, apart from the overall scale E_R, depends only on $\epsilon = \Omega_p/\Omega_c$. For $\epsilon \ll 1$, $V_{na}(x)$ is a sequence of potential hills with spacing $\lambda/2$, width $\ell \equiv \epsilon\lambda/2\pi \ll \lambda/2$ and height $E_R/\epsilon^2 \gg E_R$ (c.f. Fig. 2b), and has for $\epsilon \ll 1$ a form reminiscent of a repulsive Kronig-Penney δ-like comb $V_{na}(x) \to \sum_n E_R\lambda/(4\epsilon)\delta(x - n\lambda/2)$ [1]. For Raman beams derived from the same laser source this potential is insensitive to both intensity and phase fluctuations. We emphasize that the mechanism behind (1) is related to nonadiabatic corrections, as described by Olshanii and Dum [27], and is conceptually different from schemes relying on a substructuring AC Stark based OLs by radio frequency or laser fields [9, 11], or in combination with DSs [10]. Fig. 2a is a plot of the BO potentials $E_{0,\pm}(x)$ for blue detuning $\Omega = \Delta > 0$ and $\epsilon = 0.16$ with parameters chosen to illustrate the main features (with similar results for red detuning). For $\Delta \gg \Omega_{c,p}$, the bright state (BS) $|E_+(x)\rangle \to \sin\alpha(x)|g_1\rangle + \cos\alpha(x)|g_2\rangle$ corresponds to the standard OL $E_+(x) \to \frac{\hbar}{4}[\Omega_p^2 + \Omega_c^2(x)]/(\Delta + \frac{i}{2}\Gamma)$ as a second order Stark shift (c.f. Fig. 2a).

To quantify the above discussion and assess the validity of the BO approximation we present now a derivation and analysis of optical potentials arising from nonadiabatic corrections to atomic motion, and effects of spontaneous emission (due to admixture of bright channels). Expanding the atomic wavefunction in the BO channels, $|\Psi(x)\rangle = \sum_\sigma \Psi_\sigma(x)|E_\sigma(x)\rangle$, results in the coupled channel equation for $\Psi_\sigma(x)$ [27, 29]. The correspond-

ing Hamiltonian is $\mathcal{H} = (-i\hbar\partial_x - A(x))^2/2m + V(x)$, where the diagonal matrix $V_{\mu\sigma}(x) = E_\sigma(x)\delta_{\mu\sigma}$ contains BO potentials (see Fig. 2). Nonadiabatic processes, coupling the BO channels, arise from the spatial variation of the internal eigenstates, $-i\hbar\partial_x |E_\sigma(x)\rangle = \sum_\mu |E_\mu(x)\rangle A_{\mu\sigma}(x)$ with scaling $A_{\mu,\sigma} \sim \hbar/\ell$ (see [32]).

We are interested in the regime of approximate adiabatic decoupling of BO channels. This requires that the separations between DS and BS are larger than the channel couplings. For the DS, the lowest order contribution from the A^2-term gives rise to the nonadiabatic (conservative) potential (1) (see Fig. 2b), with consistency requirement $V_{na}(x) \ll \min|E_\pm(x)|$. We discuss this by setting the external potential $V(x) = V_L(x) = 0$, and studying the 1D bandstructure for the Λ-scheme of Fig. 1b. We compare below the results for (i) the single-channel DS potential $V_{na}(x)$ with (ii) the exact diagonalization of the (non-Hermitian) Hamiltonian H, using a Bloch ansatz $\Psi(x) = e^{iqx}u_{n,q}(x)$ with quasimomentum q to obtain the (complex) energies $\epsilon_{n,q}$. In the first case we have a unit cell $\lambda/2$ and thus a Brillouin zone $|q| < 2\pi/\lambda$, while H has periodicity λ, and thus $|q| < \pi/\lambda$, so that the bands of the first case appear as 'folded back' in the second case (see Figs. 2c,d,e).

For the DS potential $V_{na}(x)$ the band structure is for $\epsilon \ll 1$ analogous to that of a Kronig-Penney model [1]. For the lowest Bloch bands $n = 1, 2\ldots$ in the DS channel 0 we obtain (see [32])

$$\epsilon^{(0)}_{n,q} \approx E_R n^2 \left\{ 1 + \frac{4\epsilon}{\pi^2}\left[1+(-1)^n \cos\frac{\pi q}{k}\right]\right\}, \; |q| \le \frac{2\pi}{\lambda} \quad (2)$$

in very good quantitative agreement with the band structure obtained from H. These bands have narrow width $\sim \epsilon$, corresponding to a hopping amplitude $J_n = 2E_R\epsilon n^2/\pi^2$ in the terminology of the tight-binding Hubbard model [2]. The energy offset of these bands $E_R n^2$ is close to the levels in the infinitely deep rectangular well of the width $\lambda/2$, with anharmonic band spacing (independent of ϵ, and thus the height of the potential). The Wannier functions associated with these bands resemble the eigenfunctions of a box potential. This is in marked contrast to the band structure in a $V(x) = V_0 \sin^2(kx)$ OL, where energies of low lying bands are harmonic oscillator-like, and the Wannier functions are strongly localized $a_L \ll \lambda/2$ (Lamb-Dicke regime) [2]. The spectroscopy of these bands could be investigated with time-of-flight, and by modulating the lattice. A discussion of this and of loading the lowest Bloch band can be found in [32].

For the DS channel 0, the nonadiabatic couplings to the bright (dissipative) BO channels $\pm$ result in a small correction $\delta\epsilon_{n,q}$ to the dispersion, which contains a imaginary part $\mathrm{Im}\,\delta\epsilon_{n,q} = -\hbar\gamma_{n,q}/2 < 0$ signalling decay of atoms in the Bloch band. Figs. 2d,e indicate the width of the lowest Bloch band $\gamma_{1,q}$, by a red shaded region around the dispersion relation $\epsilon_{1,q}$, as obtained from a numerical solution of the coupled channel equations. The parameters are chosen to illustrate the limits of a 'large' and

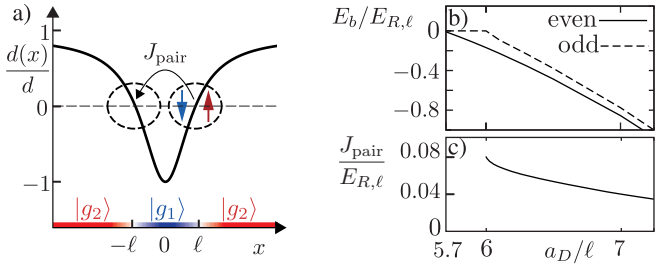

FIG. 3. (Color online) a) Position-dependent dipole moment $d(x)/d$, for $-d_1 = d_2 = d$. Molecules exist as bound states of two atoms due to dipolar attraction at the interfaces, where $d(x)$ changes sign. b) Bound state energies E_b, and c) hopping amplitude $J_{\rm pair}$ of molecules between the two interfaces for $\epsilon = 0.1$ in units of $E_{R,\ell} \equiv \hbar^2/2m\ell^2 = E_R/\epsilon^2$.

'small' decay width Γ (see [32]). We note that in both cases $\gamma_{1,q} \ll J_1$, i.e. dissipative corrections are typically very small, while $\gamma_{1,q}$ shows a nontrivial q-dependence. In Fig. 2d we can parametrize

$$\gamma_{1,q} \approx \gamma_1 \sin^2(\pi q/2k), \quad |q| \le \frac{2\pi}{\lambda} \quad (3)$$

(see [32]), where for the lowest Bloch band the decay increases with q (Fig. 2d) - something we expect from a STIRAP scenario [17], where faster atomic motion leads to a stronger violation of adiabaticity and thus depopulation of the DS. In contrast, Fig. 2e shows the appearance of *resonances* in q: as discussed in [32] these appear when for a given $q = q_\star$ the energies in the dark channel 0 becomes energetically degenerate with energies in the bright open channel $-$, $\epsilon^{(0)}_{n,q_\star} \approx \mathrm{Re}\,\epsilon^{(-)}_{n,q_\star+k}$. With increasing Γ relative to the strength of the nonadiabatic couplings these resonance get successively washed out, transitioning to the generic behavior of Fig. 2d. We refer to [32] for a detailed discussion of $\gamma_{n,q}$, and in particular scaling with system parameters.

Returning to Fig. 1a we point out that the above discussion can be generalized to DSs in 2D and 3D configurations. Thus we can replace $\Omega_c(x) \to \Omega_c(x,y)$ and $V_L(x) \to V_L(x,y)$, while preserving the existence of a DS $|E_0(x,y)\rangle$, allowing to add a (standard) OL for motion in the y-direction, or the realization of an atomic double wire with separation ℓ.

We now turn to a study of quantum many-body physics, and discuss as an illustrative example motion of two atoms confined in the subwavelength structure of Fig. 1, and interacting via magnetic dipolar interactions. The validity of (1) in a many-body Schrödinger equation will be discussed below. We assume that the two-body physics can be modeled by the external motion of each atom governed by $V_L(x) + V_{na}(x)$, while the internal state is the BO channel $|E_0(x)\rangle$, with the unique feature of an x-dependent internal state (see bottom of Fig. 1a). We consider two ground states (spins) with associated magnetic dipole moments d_1, d_2, oriented according to a quantization axis defined by an external

magnetic field, so that each atom acquires an effective position-dependent dipole moment, $d(x) = d_1 \cos^2 \alpha(x) + d_2 \sin^2 \alpha(x)$. Fig. 3a is a plot of this dipole moment for a choice of states with $-d_1 = d_2 \equiv d$, with the spatial variation of $|E_0(x)\rangle$ now imprinted as a variation of $d(x)$ on the scale ℓ. The magnetic (dipolar) interactions between the atoms is thus modulated by this spatial dependence. There are two generic situations, the first (i) with the dipole moments oriented along x, and the second (ii) with dipole oriented perpendicular. In the first case, two atoms on opposite sides of the barrier in the double layer attract each other in a head-to-tail configuration. For the case of electric dipole moments as realized with polar molecules, stored in a 2D double layer from a OL with $\lambda/2$ separation, the formation of bound states as building block for quantum phases has been studied [33–36]. Here we note that this physics of strong interactions becomes accessible, when the dipolar length, $a_D = md^2/\hbar^2$ [18, 19] characterizing the dipolar interactions [**?**], is comparable to the average distance between the atoms (here $\sim a_L$ with $\ell \ll a_L \ll \lambda_L$).

Instead, we focus here on physics of perpendicular dipole moments (ii) at the *interface* between the spin structure, $|g_1\rangle \leftrightarrow |g_2\rangle$, as shown in Fig. 3. If the dipoles are oriented perpendicular to x, atoms on opposite sites of the interface attract each other, thus allowing for the formation of a bound state as a 'domain wall' molecule. The situation is illustrated by the following two-particle Hamiltonian (see [32] for detailed description):

$$H = \sum_{i=1,2} \left[-\frac{\hbar^2 \partial_{x_i}^2}{2m} + V_{na}(x_i) \right] + \frac{d(x_1) d(x_2)}{|x_1 - x_2|^3} \qquad (4)$$

with $d(x)$ modulated on the scale ℓ, assuming strong confinement $\ell_\perp < \ell$ in the transverse plane (and setting $V_L = 0$). According to Fig. 3 we find that the requirement for a bound state of size ℓ to form is $a_D/\ell \sim 6$ [37–39], where the 'domain wall' molecules sit on the slope of the nonadiabatic potential. These molecules exist at both the left and right interfaces $\pm\ell$, and can hop between them, realizing a double layer with subwavelength distance. The (potentially large) amplitude $J_{\rm pair}$ for hopping is reflected as a hybridization of molecular orbitals on the left and right interfaces, seen in Fig. 3 as a splitting between the even and odd states. We can also obtain *trimers* as bound states of three atoms, where two spin-up dipoles sit to the left (right) of $-\ell$ ($+\ell$) and a spin-down in the middle.

From an atomic physics point of view, a Λ-scheme and a nonadiabatic DS potential can be realized with both Alkali and Alkaline Earth atoms, where two ground states are chosen from a Zeeman or hyperfine manifold. Remarkably, these nonadiabatic potentials exist, on the level of single-atom physics, as *conservative* optical potentials even *on-resonance* ($\Delta = 0$) and for short lived excited states (but still $\Omega_{c,p} \gg \Gamma$). In going off-resonance the nonadiabatic conservative potential will persist albeit with an increasing requirement for laser power to satisfy the adiabaticity requirement, in particular $V_{na}(0) < \frac{\hbar}{4}\Omega_p^2/\Delta$ ($\Omega_p \ll \Delta$) for $\Delta > 0$ as shown in Figs. 2a,b. With increasing detuning the three-level model will eventually break down, and the coupling to several excited states may become important. This situation parallels the challenges in realizing spin-dependent OLs [40–43], and spin-orbit coupling in Λ-systems with Alkali atoms [44–51], where the electronic spin-flip implicit in coupling two ground states via Raman transition is suppressed for detunings larger than the fine structure splitting of the excited state. We note, however, the encouraging prospects provided by Lanthanides in realizing spin-orbit couplings [19, 52, 53] and synthetic gauge fields [54, 55]. In a many-atom context, going to off-resonant laser excitation is a necessary requirement to suppress inelastic collision channels (involving laser excitation at the Condon point), and we expect a similar requirement here. As discussed in the context of polar molecules, long range repulsive dipolar interactions in combination with low-dimensional trapping (1D or 2D) can provide a shield in atom-atom collisions at low energies [**?**], thus suppressing inelastic loss and instabilities from short range physics [56].

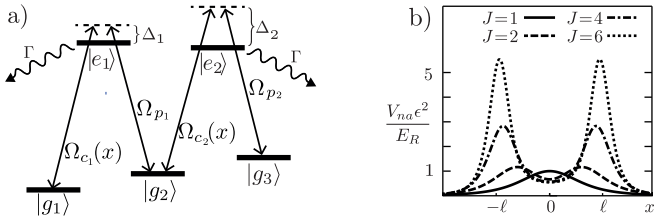

FIG. 4. a) Atomic zig-zag (double-Λ) configuration with $\Omega_{c_i}(x)$ strong standing waves and Ω_{p_i} weak probe beams, and b) the corresponding *nonadiabatic optical potentials* on the subwavelength scale $\ell \ll \lambda$ for an atomic angular momentum $J_g = J_e \equiv J$ transition, where the Zeeman levels are coupled by circularly polarized laser fields. With increasing J a double barrier structure develops.

To conclude, Λ-type configurations with nonadiabatic DS optical potentials [57] are readily generalized to zig-zag configurations as in Fig. 4a (see also [32]). This yields a *double-peaked structure* on the scale ℓ as in Fig. 4b. These ideas enable writing complex spatial spin patterns [10] and associated landscapes of nonadiabatic potentials. On the many-atom level spatially varying internal structures result in *position-dependent* interparticle interactions. This provides a novel setting for many-body atomic systems, illustrated here for magnetic dipole-dipole interactions, and poses interesting questions as quantum chemistry in atomic collisions at subwavelength distances.

ACKNOWLEDGMENTS

We thank J. Budich, L. Chomaz, J. Dalibard, M. Dalmonte, F. Ferlaino, R. Grimm, T. Pfau, and T. Porto for

helpful comments. Work at Innsbruck is supported by the ERC Synergy Grant UQUAM, the Austrian Science Fund through SFB FOQUS, and EU FET Proactive Initiative SIQS. H. P. was supported by the NSF through a grant for the Institute for Theoretical Atomic, Molecular, and Optical Physics at Harvard University and the Smithsonian Astrophysical Observatory.

[1] D. Guéry-Odelin and C. Cohen-Tannoudji, *Advances in Atomic Physics* (World Scientific, 2011).
[2] M. Lewenstein, A. Sanpera, and V. Ahufinger, *Ultracold Atoms in Optical Lattices: Simulating quantum many-body systems* (OUP Oxford, 2012).
[2] I. Bloch, J. Dalibard, and W. Zwerger, Rev. Mod. Phys. **80**, 885 (2008).
[4] R. Mitsch, C. Sayrin, B. Albrecht, P. Schneeweiss, and A. Rauschenbeutel, Nat. Commun. **5** (2014).
[5] J. Thompson, T. Tiecke, N. de Leon, J. Feist, A. Akimov, M. Gullans, A. Zibrov, V. Vuletić, and M. Lukin, Science **340**, 1202 (2013).
[6] A. González-Tudela, C.-L. Hung, D. E. Chang, J. I. Cirac, and H. Kimble, Nature Photon. **9**, 320 (2015).
[7] D. E. Chang, J. D. Thompson, H. Park, V. Vuletić, A. S. Zibrov, P. Zoller, and M. D. Lukin, Phys. Rev. Lett. **103**, 123004 (2009).
[8] M. Gullans, T. G. Tiecke, D. E. Chang, J. Feist, J. D. Thompson, J. I. Cirac, P. Zoller, and M. D. Lukin, Phys. Rev. Lett. **109**, 235309 (2012).
[9] W. Yi, A. Daley, G. Pupillo, and P. Zoller, New J. Phys. **10**, 073015 (2008).
[10] M. Kiffner, J. Evers, and M. S. Zubairy, Phys. Rev. Lett. **100**, 073602 (2008).
[11] S. Nascimbene, N. Goldman, N. R. Cooper, and J. Dalibard, Phys. Rev. Lett. **115**, 140401 (2015).
[12] G. Ritt, C. Geckeler, T. Salger, G. Cennini, and M. Weitz, Phys. Rev. A **74**, 063622 (2006).
[13] B. Brezger, T. Schulze, P. Schmidt, R. M. T. Pfau, and J. Mlynek, Europhys. Lett. **46**, 148 (1999).
[14] T. Salger, C. Geckeler, S. Kling, and M. Weitz, Phys. Rev. Lett. **99**, 190405 (2007).
[15] N. Lundblad, P. J. Lee, I. B. Spielman, B. L. Brown, W. D. Phillips, and J. V. Porto, Phys. Rev. Lett. **100**, 150401 (2008).
[16] M. Lukin, Rev. Mod. Phys. **75**, 457 (2003).
[17] N. V. Vitanov, A. A. Rangelov, B. W. Shore, and K. Bergmann, arXiv preprint arXiv:1605.00224 (2016).
[18] S. Baier, M. Mark, D. Petter, K. Aikawa, L. Chomaz, Z. Cai, M. Baranov, P. Zoller, and F. Ferlaino, Science **352**, 201 (2016).
[19] N. Q. Burdick, Y. Tang, and B. L. Lev, arXiv:1605.03211 (2016).
[20] H. Kadau, M. Schmitt, M. Wenzel, C. Wink, T. Maier, I. Ferrier-Barbut, and T. Pfau, Nature **530**, 194 (2016).
[21] I. Ferrier-Barbut, H. Kadau, M. Schmitt, M. Wenzel, and T. Pfau, Phys. Rev. Lett. **116**, 215301 (2016).
[22] A. de Paz, A. Sharma, A. Chotia, E. Maréchal, J. H. Huckans, P. Pedri, L. Santos, O. Gorceix, L. Vernac, and B. Laburthe-Tolra, Phys. Rev. Lett. **111**, 185305 (2013).
[23] C. Gardiner and P. Zoller, in *The Quantum World of Ultra-Cold Atoms and Light Book II: The Physics of Quantum-Optical Devices* (World Scientific, 2015) pp. 1–524.
[24] A. V. Gorshkov, L. Jiang, M. Greiner, P. Zoller, and M. D. Lukin, Phys. Rev. Lett. **100**, 093005 (2008).
[25] This is in contrast to spin-orbit coupling schemes based on running wave laser configurations with Λ-systems [49].
[26] A. P. Kazantsev, G. Surdutovich, and V. Yakovlev, *Mechanical action of light on atoms* (World Scientific, 1990).
[27] R. Dum and M. Olshanii, Phys. Rev. Lett. **76**, 1788 (1996).
[28] S. K. Dutta, B. K. Teo, and G. Raithel, Phys. Rev. Lett. **83**, 1934 (1999).
[29] J. Ruseckas, G. Juzeliūnas, P. Öhberg, and M. Fleischhauer, Phys. Rev. Lett. **95**, 010404 (2005).
[30] K. Bergmann, N. V. Vitanov, and B. W. Shore, J. Chem. Phys. **142**, 170901 (2015).
[1] E. Merzbacher, *Quantum Mechanics* (Wiley, 1998).
[32] See Appendices.
[33] D.-W. Wang, M. D. Lukin, and E. Demler, Phys. Rev. Lett. **97**, 180413 (2006).
[34] A. Pikovski, M. Klawunn, G. V. Shlyapnikov, and L. Santos, Phys. Rev. Lett. **105**, 215302 (2010).
[35] M. A. Baranov, A. Micheli, S. Ronen, and P. Zoller, Phys. Rev. A **83**, 043602 (2011).
[36] M. A. Baranov, M. Dalmonte, G. Pupillo, and P. Zoller, Chem. Rev. **112**, 5012 (2012).
[37] B. Yan, S. A. Moses, B. Gadway, J. P. Covey, K. R. Hazzard, A. M. Rey, D. S. Jin, and J. Ye, Nature **501**, 521 (2013).
[38] S. A. Moses, J. P. Covey, M. T. Miecnikowski, B. Yan, B. Gadway, J. Ye, and D. S. Jin, Science **350**, 659 (2015).
[39] For transverse confinement $\ell_\perp$ with a non-resonant optical lattice we note the condition $\ell > \ell_\perp$.
[40] O. Mandel, M. Greiner, A. Widera, T. Rom, T. W. Hänsch, and I. Bloch, Phys. Rev. Lett. **91**, 010407 (2003).
[41] P. J. Lee, M. Anderlini, B. L. Brown, J. Sebby-Strabley, W. D. Phillips, and J. V. Porto, Phys. Rev. Lett. **99**, 020402 (2007).
[42] P. Soltan-Panahi, J. Struck, P. Hauke, A. Bick, W. Plenkers, G. Meineke, C. Becker, P. Windpassinger, M. Lewenstein, and K. Sengstock, Nat. Phys. **7**, 434 (2011).
[43] H.-N. Dai, B. Yang, A. Reingruber, X.-F. Xu, X. Jiang, Y.-A. Chen, Z.-S. Yuan, and J.-W. Pan, Nat. Phys. (2016).
[44] Y. J. Lin, K. Jiménez-García, and I. B. Spielman, Nature **471**, 83 (2011).
[45] P. Wang, Z.-Q. Yu, Z. Fu, J. Miao, L. Huang, S. Chai, H. Zhai, and J. Zhang, Phys. Rev. Lett. **109**, 095301 (2012).
[46] L. W. Cheuk, A. T. Sommer, Z. Hadzibabic, T. Yefsah, W. S. Bakr, and M. W. Zwierlein, Phys. Rev. Lett. **109**, 095302 (2012).
[47] B. K. Stuhl, H. I. Lu, L. M. Aycock, D. Genkina, and I. B. Spielman, Science **349**, 1514 (2015).
[48] L. Huang, Z. Meng, P. Wang, P. Peng, S.-L. Zhang, L. Chen, D. Li, Q. Zhou, and J. Zhang, Nat. Phys. **12**, 540 (2016).

[49] V. Galitski and I. B. Spielman, Nature **494**, 49 (2013).
[50] J. Dalibard, F. Gerbier, G. Juzeliūnas, and P. Öhberg, Rev. Mod. Phys. **83**, 1523 (2011).
[51] N. Goldman, J. C. Budich, and P. Zoller, Nat. Phys. **12**, 639 (2016).
[52] X. Cui, B. Lian, T.-L. Ho, B. L. Lev, and H. Zhai, Phys. Rev. A **88**, 011601 (2013).
[53] M. Mancini, G. Pagano, G. Cappellini, L. Livi, M. Rider, J. Catani, C. Sias, P. Zoller, M. Inguscio, M. Dalmonte, and L. Fallani, Science **349**, 1510 (2015).
[54] S. Nascimbène, J. Phys. B **46**, 134005 (2013).
[55] M. L. Wall, A. P. Koller, S. Li, X. Zhang, N. R. Cooper, J. Ye, and A. M. Rey, Phys. Rev. Lett. **116**, 035301 (2016).
[56] A. Micheli, Z. Idziaszek, G. Pupillo, M. A. Baranov, P. Zoller, and P. S. Julienne, Phys. Rev. Lett. **105**, 073202 (2010).
[57] Note added: After submission of the present work as arXiv:1607.07338 we have become aware of arXiv:1609.01285, Subwavelength-width optical tunnel junctions for ultracold atoms by F. Jendrzejewski et al., which overlaps with the first part of the present manuscript.

SUPPLEMENTAL MATERIAL

Appendix A: Born-Oppenheimer approach

Here we present details of the Born-Oppenheimer (BO) approach used for the analysis of the Λ-system described in the main text. In the bare atomic basis $|g_1\rangle$, $|e\rangle$, and $|g_2\rangle$, the Hamiltonian of the system reads

$$H = -\frac{\hbar^2\partial_x^2}{2m} + \hbar \begin{pmatrix} 0 & \Omega_c(x)/2 & 0 \\ \Omega_c(x)/2 & -\tilde{\Delta} & \Omega_p/2 \\ 0 & \Omega_p/2 & 0 \end{pmatrix} \quad \text{(A1)}$$

with $\tilde{\Delta} = \Delta + i\Gamma/2$ This Hamiltonian is non-Hermitian (for $\Gamma \neq 0$) and has complex eigenvalues and a bi-orthogonal set of the left and right eigenstates. In the BO approximation we drop the kinetic energy term, and corresponding right (adiabatic) eigenstates are the dark $|E_0\rangle$ and bright $|E_\pm\rangle$ eigenstates

$$|E_0\rangle = -\cos\alpha\,|g_1\rangle + \sin\alpha\,|g_2\rangle\,,$$
$$|E_\pm\rangle = N_\pm\left\{\epsilon_\pm\,|e\rangle + [\sin\alpha\,|g_1\rangle + \cos\alpha\,|g_2\rangle]\right\}$$

with $\alpha(x) = \arctan[\Omega_c(x)/\Omega_p]$ have eigenenergies $E_0 = 0$ and $E_\pm(x)$, respectively. Here $\epsilon_\pm = 2E_\pm(x)/E(x)$ with $E(x) = \hbar\sqrt{\Omega_p^2 + \Omega_c(x)^2}$, and $N_\pm = (1+\epsilon_\pm^2)^{-1/2}$. We emphasize that these eigenstates and eigenenergies depend parametrically on the position x.

Straightforward calculations of the derivatives of the eigenstates $|E_\sigma(x)\rangle$ for $\sigma = 0, \pm$ in the expression $-i\hbar\partial_x\,|E_\sigma\rangle = \sum_\mu |E_\mu\rangle\, A_{\mu\sigma}$ give

$$A = -i\hbar\alpha' \begin{pmatrix} 0 & -N_+ & -N_- \\ N_+ & 0 & -C \\ N_- & C & 0 \end{pmatrix}$$

with

$$C = \widetilde{\Delta}\frac{\Omega_c(x)}{2\Omega_p}\frac{E(x)}{E(x)^2 + \widetilde{\Delta}^2},$$

such that the Hamiltonian H for the wave functions $\Psi_\sigma(x)$ reads

$$\mathcal{H} = -\frac{\hbar^2\partial_x^2}{2m} + \begin{pmatrix} 0 & 0 & 0 \\ 0 & E_+ & 0 \\ 0 & 0 & E_- \end{pmatrix} \quad \text{(A2)}$$

$$+ \frac{\hbar^2(\alpha')^2}{2m} \begin{pmatrix} 1 & 0 & 0 \\ 0 & N_+^2 + C^2 & 0 \\ 0 & 0 & N_-^2 + C^2 \end{pmatrix} \quad \text{(A3)}$$

$$- \frac{i\hbar}{2m}\left(\partial_x A + A\partial_x\right) \quad \text{(A4)}$$

$$- \frac{\hbar^2(\alpha')^2}{2m} \begin{pmatrix} 0 & CN_- & -CN_+ \\ CN_- & 0 & -N_+N_- \\ -CN_+ & -N_+N_- & 0 \end{pmatrix}. \quad \text{(A5)}$$

The Hamiltonian is naturally split into a diagonal part $\mathcal{H}_D$ (the first two lines) which determines the BO band-structures for the dark and bright channels, and off-diagonal terms $\mathcal{H}_C$ (the last two lines) determining the coupling between them. The coupling contains $\alpha'(x)$ and, therefore, mostly takes place in the narrow regions with the width $\Delta x \sim \epsilon/k \sim \epsilon\lambda$ around the points $x_s = \pi s/k = s\lambda/2$ with integer s. The strength of the coupling is essentially determined by the ratio κ of the strength of the non-adiabatic potential $V_{na}(x=0) = E_R/\epsilon^2$ and the energy gap between the dark and the bright states. The latter depends on the detuning and is of the order of Ω_p for the resonant case $\Delta = 0$, and $\Omega_p^2/|\Delta|$ for the off-resonant case with large Δ. As a result, for the considered case $\kappa \ll 1$, where $\kappa = E_R/\Omega_p\epsilon^2$ for $\Delta = 0$ and $\kappa = E_R\,|\Delta|\,/\Omega_p^2\epsilon^2$ for large $|\Delta|$, the couplings are small justifying the perturbative approach in the main text.

Appendix B: Band structure in the Born-Oppenheimer approximation

In the following we provide details on the band structure of the dark and bright channels in the BO approximation. We first analyze the case of uncoupled BO channels and then discuss the effects of non-adiabatic couplings between them.

The diagonal Hamiltonian describing uncoupled BO dark and bright channels reads

$$\mathcal{H}_D = -\frac{\hbar^2\partial_x^2}{2m} + \begin{pmatrix} V_{na}(x) & 0 & 0 \\ 0 & E_+(x) & 0 \\ 0 & 0 & E_-(x) \end{pmatrix},$$

where for $\kappa \ll 1$ we neglect the nonadiabatic contribution to the bright channels.

The second term in $\mathcal{H}_D$ is periodic with $\lambda/2 = \pi/k$, and, therefore, the single-particle eigenstates are Bloch wave functions $\psi_{n,q}(x)$ characterized by the quasimomentum q in the Brillouin zone, $q \in [-k, k]$, such that $\psi_{n,q}(x + \lambda/2) = \exp(iq\lambda/2)\psi_{n,q}(x)$, and by the band index $n = 1, 2, \ldots$, with the corresponding eigenenergies $\epsilon_{n,q}$ forming the band structure. Note that the periodicity of the Hamiltonian $\mathcal{H}$ is $2\pi/k = \lambda$ (because of the coupling terms proportional to α'), while the diagonal part $\mathcal{H}_D$ has periodicity $\pi/k = \lambda/2$ (α' changing sign under $x \to x + \pi/k$). For this reason, for describing the band structure we will use both the Brillouin zone (BZ) of $\mathcal{H}_D$ with quasimomenta $q \in [-k, k]$ and the (folded) Brillouin zone (FBZ) of $\mathcal{H}$ with $\overline{q} \in [-k/2, k/2]$, with the obvious mapping between them: $\overline{q} = q$ for $q \in [-k/2, k/2]$ and $\overline{q} = q - k$ or $\overline{q} = q + k$ for $q \in [k/2, k]$ or $q \in [-k, -k/2]$, respectively. Under this folding, the dispersion relation $\epsilon_{n,q}$ for the Bloch states in BZ is mapped on the *continuous* dispersion relation $\overline{\epsilon}_{n,\overline{q}}$ for states in FBZ, which has two branches $\epsilon_{n,\overline{q}}$ and $\epsilon_{n,\overline{q}+k}$ continuously matching at $\overline{q} = \pm k/2$.

1. Band structure of the dark-state channel 0

The part of the Hamiltonian $\mathcal{H}_D$ for the dark-state

$$\mathcal{H}_0 = -\frac{\hbar^2\partial_x^2}{2m} + V_{na}(x),$$

is Hermitian and describes the motion of particle in the periodic (with π/k) set of sharp δ-like potential peaks of the width $\Delta x \sim \epsilon/k \ll \pi/k$ around points $x_n = (\pi/k)n$, and height $E_R/\epsilon^2 \gg E_R$ (analog of the Kronig-Penney model). In this case, the structure of the low-energy bands with $\epsilon_{n,q} \ll \hbar^2/m(\Delta x)^2$ is fully determined by the transmission amplitude $t(E)$ through a single barrier [1]. The corresponding relation between the quasimomentum q and the energy $\epsilon_{n,q}$ reads

$$\cos \pi q/k = \frac{1}{2}\left[\frac{1}{t^*(\epsilon_{n,q})}e^{i\pi Q/k} + \frac{1}{t(\epsilon_{n,q})}e^{-i\pi Q/k}\right], \quad \text{(B1)}$$

where $Q = \sqrt{2m\epsilon_{n,q}/\hbar^2}$ and we took into account that the length of the unit cell is π/k.

To find the transition amplitude $t(E)$ as a function of energy E we have to solve the scattering problem for a single barrier located at $x = 0$, which for $\epsilon \ll 1$ can be approximated as

$$V_{na}(x) \approx V(x) = E_R\frac{\epsilon^2}{[\epsilon^2 + (kx)^2]^2}. \quad \text{(B2)}$$

The corresponding Schrödinger equation reads

$$\left[-\frac{\hbar^2\partial_x^2}{2m} + V(x)\right]\psi(x) = E\psi(x),$$

and the boundary conditions are

$$\psi(x \to -\infty) = e^{iQx} + r(E)e^{-iQx},$$
$$\psi(x \to +\infty) = t(E)e^{iQx},$$

where $Q = \sqrt{2mE/\hbar^2}$. In the units $s = kx/\epsilon$ we get

$$\left[-\frac{d^2}{ds^2} + \frac{1}{(1+s^2)^2}\right]\psi(s) = \epsilon^2\left(\frac{Q}{k}\right)^2\psi(s).$$

Inside the barrier ($|s| \ll 1/\sqrt{\epsilon}$ or $|x| \ll \sqrt{\epsilon}/k$) we can neglect the right-hand-side and reduce the equation to the form

$$\left[-\frac{d^2}{ds^2} + \frac{1}{(1+s^2)^2}\right]\psi(s) = 0$$

which general solution is

$$\psi(s) = \sqrt{1+s^2}(A + B\arctan s), \quad |s| \ll \frac{1}{\sqrt{\epsilon}}. \quad \text{(B3)}$$

Outside the barrier ($|s| \gg 1/\sqrt{\epsilon}$), the potential is negligible, and the resulting equation

$$-\frac{d^2}{ds^2}\psi(s) = \epsilon^2\left(\frac{Q}{k}\right)^2\psi(s)$$

has general solution

$$\psi(s) = C\exp\left(\frac{i\epsilon Qs}{k}\right) + D\exp\left(-\frac{i\epsilon Qs}{k}\right), \quad |s| \gg \frac{1}{\sqrt{\epsilon}}. \quad \text{(B4)}$$

For the scattering problem we have to set $C = 1$, $D = r(E)$ for large negative s, and $C = t(E)$, $D = 0$ for large positive s, respectively. After matching Eqs. (B3) and (B4) at $|s| = |s_*| \sim 1/\sqrt{\epsilon}$ ($1 \ll |s_*| \ll 1/\epsilon$) where the barrier potential is comparable with the energy, we obtain

$$t(E) = -\left(1 - i\frac{\pi}{2\epsilon}\frac{k}{Q}\right)^{-1} \quad \text{(B5)}$$

This result, although being similar, is not identical with that for the δ-functional potential $V_\delta(x) = (\hbar^2/2m)(\pi k/2\epsilon)\delta(x)$ of the strength $\int dx V(x)$. The latter is equivalent to imposing the boundary conditions at the origin

$$\psi_+ - \psi_- = 0,$$
$$\psi'_+ - \psi'_- = \frac{\pi k}{4\epsilon}(\psi_+ + \psi_-),$$

where $\psi_\pm = \psi(\pm 0)$ and $\psi'_\pm = \partial_x\psi(\pm 0)$ are the values of the wave function and its derivative, respectively, on the left ($x = -0$) and on the right ($x = +0$) of the δ-functional barrier $V_\delta(x)$. Similar boundary conditions can also be written for the potential $V(x)$, although they are applicable only for the wave functions with energies $E \ll E_R/\epsilon^2$: After writing the asymptotic of the wave function in the form $\psi(x) \to \psi_\pm + \psi'_\pm x$ for $x \sim \pm\sqrt{\epsilon}/k$ and matching them with the asymptotic of Eqs. (B3), we obtain

$$\psi_+ + \psi_- = 0,$$
$$\psi'_+ + \psi'_- = -\frac{\pi k}{2\epsilon}(\psi_+ - \psi_-).$$

To demonstrate the difference between the two sets of boundary conditions, we present the result for the transition amplitude $t_\delta(E)$ through the potential $V_\delta(x)$:

$$t_\delta(E) = \left(1 + i\frac{\pi}{4\epsilon}\frac{k}{Q}\right)^{-1}, \quad \text{(B6)}$$

which has similar scaling for $Q \to 0$ as $t(E)$ but different coefficient and subleading terms.

2. Dispersion relation for the Bloch bands

With the expression (B5) for the transition amplitude, Eq. (B1) for the dispersion relation for the Bloch bands reads

$$\cos \pi q/k = -\cos(\pi Q/k) + \frac{\pi k}{2Q\epsilon}\sin(\pi Q/k).$$

For $\epsilon \ll 1$, the solutions for Q are located near the points kn, $n = 1, 2, \ldots$ After linearizing around these points we obtain for $1 \le n < \epsilon^{-1}$

$$Q_n(q) \approx kn \left\{ 1 + \frac{2\epsilon}{\pi^2} \left[1 + (-1)^n \cos\frac{\pi q}{k} \right] \right\}$$

and $\hbar^2 Q_n^2(q)/2m$ gives Eq. (2) in the main text for the dispersion of the lower Bloch bands in the dark-state channel. Note that if we approximate the non-adiabatic potential with the periodic set of δ-functions [in other words, use $t_\delta(E)$, Eq. (B6), instead of $t(E)$ in Eq. (B5)], the expression (2) in the main text for the dispersion relation changes into

$$\epsilon_{n,q}^{(\delta)} \approx E_R n^2 \left\{ 1 - \frac{8\epsilon}{\pi^2} \left[1 - (-1)^n \cos\frac{\pi q}{k} \right] \right\}. \qquad \text{(B7)}$$

a. Wave functions for the Bloch band

Eqs. (B3) and (B4) can also be used for finding the Bloch wave functions $\psi_{n,q}(x)$, as we demonstrate for the lowest band $n = 1$ with energies $\epsilon_{1,q} \simeq E_R$. The wave functions for higher bands can be found in the same way, and the answer will be given at the end of this section). The expression for $\psi_{1,q}(x)$ will be given for $q \in [-k, k]$ and $x \in [-\pi/2k, \pi/2k]$. For other values of x, the wave function can be calculated from the relation $\psi_{1,q}(x + \pi/k) = \exp(i\pi q/k)\psi_{1,q}(x)$.

With the approximation $V_{na}(x) \approx V(x)$, Eq. (B2), and new variable $s = kx/\epsilon \in [-\pi/2\epsilon, \pi/2\epsilon]$, the equation for $\psi_{1,q}(s)$ reads

$$\left[-\frac{d^2}{ds^2} + \frac{1}{(1+s^2)^2} \right] \psi_q(s) = \epsilon^2 \psi_{1,q}(s),$$

where we used the fact that $\epsilon_{1,q} \simeq E_R$. The two solutions (B3) and (B4) have to be matched at $|s_*| \sim 1/\sqrt{\epsilon}$ in such a way that

$$\frac{\psi_{1,q}(\pi/2\epsilon)}{\psi_{1,q}(-\pi/2\epsilon)} = \exp(i\pi q/k). \qquad \text{(B8)}$$

This gives in the original variable $x \in [-\pi/2k, \pi/2k]$

$$\psi_{1,q}(x) \approx N\sqrt{\epsilon^2 + \sin^2(kx)} \left[\cos\left(\frac{\pi q}{2k}\right) + \frac{2i}{\pi} \sin\left(\frac{\pi q}{2k}\right) \arctan\left(\frac{\tan(kx)}{\epsilon}\right) \right] \qquad \text{(B9)}$$

$$= \cos\left(\frac{\pi q}{2k}\right) \psi_0(x) + i \sin\left(\frac{\pi q}{2k}\right) \psi_\pi(x) \qquad \text{(B10)}$$

for $q \in [-k, k]$, where N is the normalization coefficient, $N \approx \sqrt{2k/\pi}$, corresponding to the unity of the integral of $|\psi_{1,q}(s)|^2$ over the unit cell $x \in [-\pi/2k, \pi/2k]$. Note the substitution $\tan(kx)/\epsilon$ instead of $s = kx/\epsilon$ in the argument of the arctan function, which provides the second independent solution [$\sim \cos(kx)$] outside the barrier in addition to $\sin(kx)$.

For the wave functions of the higher bands similar considerations give the following approximate expression:

$$\psi_{n,q}(x) \approx N_n \sqrt{\epsilon^2 + \sin^2 z} \left[-\frac{\sin(nz)}{\sin z} \left(\frac{z}{i|z|} \right)^{n+1} e^{i\frac{\pi q}{2k}\frac{z}{|z|}} - \frac{2in}{\pi} \cos\left(\frac{\pi q}{2k} - \frac{\pi n}{2}\right) \cos(nz) \arctan\left(\frac{\epsilon}{\tan z}\right) \right], \qquad \text{(B11)}$$

where $z \equiv kx \in [-\pi/2, \pi/2]$, $q \in [-k, k]$, and the band index n should satisfy the condition $n\epsilon \ll 1$.

b. Band structure of the bright-state channels ±

The Hamiltonians for the bright-state BO channels

$$\mathcal{H}_\pm = -\frac{\hbar^2 \partial_x^2}{2m} + E_\pm(x)$$

describe the motion in the complex potentials of local bright-state eigenenergies.

For the near-resonant case $\Delta = 0$, we have

$$E_\pm(x) \approx \pm\frac{1}{2}E(x) - \frac{i\Gamma}{4},$$

while for the off-resonant case $|\Delta| \gg \Omega_c$

$$E_+(x) \approx \frac{E^2(x)}{4\widetilde{\Delta}} \approx \frac{E^2(x)}{4\Delta}\left(1 - i\frac{\Gamma}{2\Delta}\right),$$
$$E_-(x) \approx -\Delta - i\frac{\Gamma}{2} - \frac{E^2(x)}{4\Delta}.$$

Note that, in contrast to $E_0(x)$, the potentials $E_\pm(x)$ have imaginary part due to the presence of the excited state $|e\rangle$ in the wave functions of the bright states. This leads to the decay of the corresponding Bloch states in the bright bands already on the level of the diagonal Hamiltonians $\mathcal{H}_\pm$, in contrast to the Bloch states for the dark state with Hermitian $\mathcal{H}_0$. The potentials $E_\pm(x)$ are the standard optical lattice potentials, giving rise to the standard band structures (see, for example, the review [2] and references therein). The resulting band structure for the off-resonant case with positive detuning and $\Gamma = 0$ is shown in Fig. 6.

Appendix C: Bloch bands of the Λ-system – numerical solution

Our numerical analysis of the system is based on the Hamiltonian (A1) written in the basis $|g_1\rangle, |g_2\rangle, |e\rangle$ and uses the Bloch ansatz $\psi_q(x) = \mathbf{u}(x)e^{iqx}$. Here $\mathbf{u}(x) = (u_{g_1}(x), u_e(x), u_{g_2}(x))^T$ is a periodic function with period λ [the periodicity of the Hamiltonian (A1)], and $q \in [-\pi/\lambda, \pi/\lambda]$ is the quasimomentum.

With this ansatz, the Schrödinger equation for the quasiperiodic Bloch function $\psi(x)$ turns into an equation for a periodic function $\mathbf{u}(x)$:

$$\left[\frac{1}{2m}\left(-i\hbar\partial_x+q\right)^2+\begin{pmatrix}0 & \Omega_c(x)/2 & 0\\ \Omega_c(x)/2 & -\widetilde{\Delta} & \Omega_p/2\\ 0 & \Omega_p/2 & 0\end{pmatrix}\right]\mathbf{u}(x)=\epsilon(q)\mathbf{u}(x) \tag{C1}$$

with q being an external parameter. Fourier expansion of the functions $u_a(x)$ with $a=g_{1,2},e$ gives

$$u_a(x)=\sum_{n=-N}^{N}\tilde{u}_{a,n}e^{in\frac{2\pi}{\lambda}x}, \tag{C2}$$

which is truncated to $|n|\leq N$, Eq. (C1) reduces the above equation to the matrix eigenvalue problem for a non-Hermitian $3(2N+1)\times 3(2N+1)$ sparse matrix.

The value N necessary for the convergence of the solution is determined by the requirement that the expansion (C2) correctly represents rapidly oscillating wave function of the bright channels, which have visible coupling to the dark channel. For $\epsilon\approx 0.1,\Omega_c,\Delta\in O(10^4)E_R$, values $N\approx 200-400$ are found to be sufficient.

Appendix D: Loading protocol for lowest Bloch band of the 'dark state' channel 0

In this section we present the details of the protocol for loading into the lowest Bloch band for the 'dark state' channel 0, referred to in the main text.

We assume a laser configuration, where the control field is switched off initially, $\Omega_c=0$, while the probe laser $\Omega_p=$ const, i.e. the dark state is simply $|g_1\rangle$). Initially, we turn on an additional off-resonant optical lattice potential $V_L(x)=V_0\cos^2(k_Lx)$ acting on the ground states. Note that this potential is chosen so that peaks of the periodic potential $V_L(x)$ at positions $n\lambda_L/2$ $(n=0,\pm1,\ldots)$ match those of $V_{na}(x)$ (we consider $k_L=k$). The protocol consists of adiabatically turning off the OL $V_L(x)$, while turning on Ω_c to its final value. The lowest Bloch band in the OL $V_L(x)$ is thus mapped to the lowest Bloch band of $V_{na}(x)$, and an atom prepared in the lowest Bloch band of $V_L(x)$ will be adiabatically transferred to the lowest band of $V_{na}(x)$. Adiabaticity during the transfer in a time period τ is guaranteed by the finite excitation gap during this process, as indicated in Fig. 5a (and similarly for gaps between the dark and the bright states). To be specific we choose a linear ramp $V_0(t)=V_0\cdot(1-t/\tau)$ and $\Omega_c(t)=\Omega_c\cdot t/\tau$, where $V_0=30E_R$.

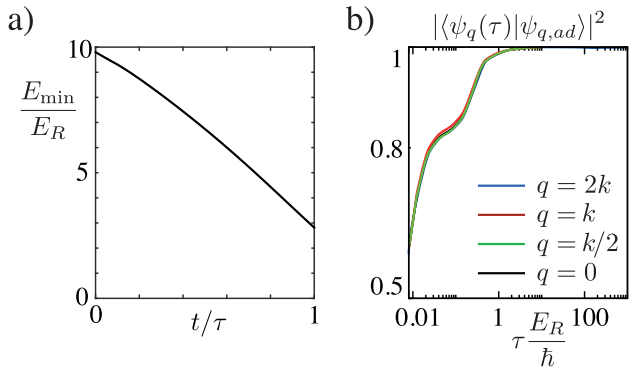

FIG. 5. (Color online) a) The finite gap between the two lowest dark-state bands during the whole loading protocol (see text). b) Overlap between the final state during the loading protocol $|\psi_q(\tau)\rangle$ Bloch band as a function of the protocol duration τ for several values of the quasimomentum q. The chosen parameters of the system are $\epsilon=0.1$, $\Omega_p=2000E_R$, $\Delta=\Gamma=0, V_0=30E_R$.

As an initial state we choose the state $|\psi_q\rangle$ with the quasimomentum q in the lowest Bloch band of the potential $V_L(x)$. The evolution of this state $|\psi_q(t)\rangle$ during the protocol is calculated using the complete Hamiltonian of the system, and Fig. 5b shows the results for the overlap (fidelity) of the final state of this evolution $|\psi_q(\tau)\rangle$ with the target state $|\psi_{q,ad}(t)\rangle$ in the lowest dark-state Bloch band in the non-adiabatic potential $V_{na}(x)$ for several values of q as a function of τ. We see that the fidelity approaches unity for τ being already few inverse recoil frequencies $\hbar/E_R$. For shorter τ, the fidelity rapidly decreases first when $\hbar/\tau$ becomes of the order of the gap between the first dark-state Bloch bands ($\sim E_R$), and then of the order of the gap to the bright states ($\sim\Omega_p$).

In conclusion, an efficient transfer protocol exists to prepare atoms in the lowest Bloch band of the 'dark state' channel 0.

Appendix E: Effects of couplings between Born-Oppenheimer channels

Here we present analytic considerations of the decay of the dark-state BO channel due to non-adiabatic couplings to the bright-state channels, supporting our numerical findings shown in Figs. 2d and 2a in the main text. We limit the discussion to the lowest dark-state Bloch band.

The dominant coupling of the dark state to the bright ones is given by Eq. (A4). Being proportional to $\alpha'(x)$ which is anti-periodic with π/k, these terms couple quasimomenta q and $q+k$ (or to $q-k=q+k-2k$). The second order correction to the energy of the lowest dark

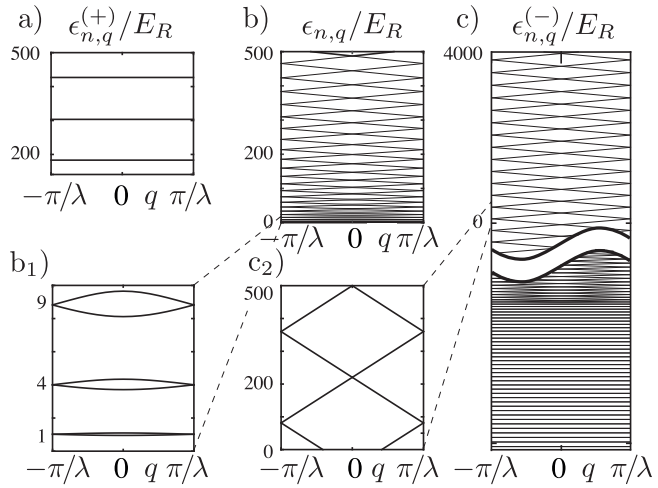

FIG. 6. Band structure for uncoupled BO dark and bright channels. Panel a) shows lowest levels for BO channel +, a ladder of (for low energies) harmonic levels tightly bound in the BO potential $E_+(x)$. Panel b) band structure for 0 channel, for BO potential V_{na} with accompanying magnification in b$_2$) of lowest few, gapped bands. Panel c) shows extent of bands for the BO channel −, from the minimum of BO − potential $E_-(x)$. through potential threshold, up to high-above-threshold regime [shown also in the accompanying magnification c$_2$)] where the particle is in almost freely-moving with a high-momentum, with a large slope of dispersion relation $\epsilon^{(-)}_{n,q}$ in c$_2$). Parameters: $\Omega_c = \Delta = 1.7\times10^4 E_R$, $\epsilon = 0.16$, and $\Gamma = 0$.

state with the quasimomentum q is

$$\delta\epsilon_{1,q} = \sum_{\sigma=\pm,n_\sigma} \frac{|M_{\sigma n}(q)|^2}{\epsilon_{1,q}(q) - \epsilon^{(\sigma)}_{n_\sigma,q+k}},$$

where $\sigma = \pm$ refers to the upper and lower bright states, $\epsilon^{(\sigma)}_{n_\sigma,q}$ are the corresponding dispersions for the n_σ-th band, and $M_{\sigma n}(q)$ are the coupling matrix elements

$$M_{\sigma n}(q) = \frac{\hbar^2}{2m}\int_{-\pi/2k}^{\pi/2k} dx\alpha'(x)N_\sigma(x) \left\{-\psi_{1,q}(x)\partial_x\psi^{(\sigma)*}_{n,q+k}(x) + \psi^{(\sigma)*}_{n,q+k}(x)\partial_x\psi_{1,q}(x)\right\}, \quad \text{(E1)}$$

where $\psi^{(\sigma)}_{n,q}(x)$ and $\psi_{1,q}(x)$ are the wave functions of the bright σn and lowest dark [see Eq. (B9)] states, respectively, and we performed integration by part in the first term.

The imaginary part of $\delta\epsilon_{1,q}$ is

$$\mathrm{Im}\,\delta\epsilon_{1,q} = \sum_{n_+} \frac{|M_{+n}(q)|^2\,\mathrm{Im}\,\epsilon^{(+)}_{n,q+n}}{[\epsilon_{1,q} - \mathrm{Re}\,\epsilon^{(+)}_{n,q+k}]^2 + [\mathrm{Im}\,\epsilon^{(+)}_{n,q+k}]^2} \quad \text{(E2)}$$

$$+ \sum_{n_-} \frac{|M_{-n}(q)|^2\,\mathrm{Im}\,\epsilon^{(-)}_{n,q+k}}{[\epsilon_{1,q} - \mathrm{Re}\,\epsilon^{(-)}_{n,q+k}]^2 + [\mathrm{Im}\,\epsilon^{(-)}_{n,q+k}]^2}, \quad \text{(E3)}$$

where we write explicitly the contributions from the upper (+) and the lower (−) bright states. Keeping in mind that both $\epsilon_{1,q}$ and $\mathrm{Im}\,\epsilon^{(+)}_{n,q+k}$ are much smaller than the energy gap to the upper bright state, the contribution $\mathrm{Im}\,\delta\epsilon_{1,q+}$ from the upper bright states can be written as

$$\mathrm{Im}\,\delta\epsilon_{1,q+} \approx \sum_{n_+} |M_{+n}(q)|^2 \frac{\mathrm{Im}\,\epsilon^{(+)}_{n,q+k}}{[\mathrm{Re}\,\epsilon^{(+)}_{n,q+k}]^2}.$$

The dominant terms come from the lowest bands which are well-described in the tight-binding approximation by using the localized states $\phi_n(x)$ in local potential wells. The coupling matrix element (E1) involves the first derivative and, as a result, the part ψ_π of the dark state wave function [see Eq. (B10)] couples to the even bands, while ψ_0 to the odd ones. One can see that the combination in the bracket in Eq. (E1) pushes the zeroes of $\phi_n(x)$ outside the center of the well for even n, and towards the center for odd n. For this reason the couplings to even n are larger, and keeping them as the sole contribution we get

$$\mathrm{Im}\,\delta\epsilon_{1,q+} \approx \sin^2(\frac{\pi q}{2k}) \sum_{\text{even } n_+} \left|m^\pi_{+n}\right|^2 \frac{\mathrm{Im}\,\epsilon^{(+)}_{n,q+k}}{[\mathrm{Re}\,\epsilon^{(+)}_{n,q+k}]^2},$$

where

$$m^\pi_{+n} = \frac{\hbar^2}{2m}\int_{-\pi/2k}^{\pi/2k} dx\alpha'(x)N_+(x) \left\{-\psi_\pi(x)\partial_x\phi_n(x) + \phi_n(x)\partial_x\psi_\pi(x)\right\}.$$

The q-dependence of the dispersion $\epsilon^{(+)}_{n,q+k}$ of the lowest bands can also be neglected, $\epsilon^{(+)}_{n,q} \approx \epsilon^{(+)}_n$, and we obtain

$$\mathrm{Im}\,\delta\epsilon_{1,q+} \approx \sin^2\left(\frac{\pi q}{2k}\right) \sum_{\text{even } n_+} \left|m^\pi_{+n}\right|^2 \frac{\mathrm{Im}\,\epsilon^{(+)}_n}{[\mathrm{Re}\,\epsilon^{(+)}_n]^2} \equiv -\frac{1}{2}\sin^2\left(\frac{\pi q}{2k}\right)\gamma_1^{(0\to+)}\left(\epsilon, \frac{\Omega_p}{E_R}, \frac{\Delta}{\Omega_p}, \frac{\Gamma}{\Omega_p}\right).$$

The contribution [see Eq. (E3)] from the lower bright state has two different parts: A resonant contribution $\mathrm{Im}\,\delta\epsilon_{1,q-\mathrm{res}}$ from the band n_0 with the states, which are resonant to the dark state for some resonant quasimomentum q_*, $\mathrm{Re}\,\epsilon^{(-)}_{n_0,q_*+k} \approx \epsilon_{1,q_*}$, and a regular one $\mathrm{Im}\,\delta\epsilon_{1,q-\mathrm{reg}}$ from the other bands with $\mathrm{Re}\,\epsilon^{(-)}_{n_0,q+k}$ being far from $\epsilon_{1,q}$. The dominant contributions to $\mathrm{Im}\,\delta\epsilon_{1,q-\mathrm{reg}}$ come from the bands with energies close to the top of the optical potential $E_-(x)$, for which the wave functions have substantial amplitudes and oscillate slowly in the coupling region $\alpha'(x) \neq 0$. In this region, the wave functions of the relevant states depend only weakly on q, such that the leading q-dependence of the coupling matrix elements is again determined by the coupling to the dark-state wave function $\psi_\pi(x)$, $M_{-n}(q) \approx \sin(\pi q/2k)M_{-n}$. The decay rates $\mathrm{Im}\,\epsilon^{(-)}_{n,q+n}$ of the relevant bright states

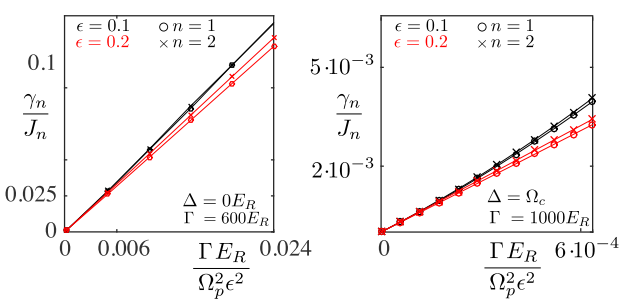

FIG. 7. (Color online) Functions γ_n determining the regular decay of the two lowest Bloch bands $n = 1, 2$ in the dark-state channel 0 for the resonant (left panel) and off-resonant (right panel) cases.

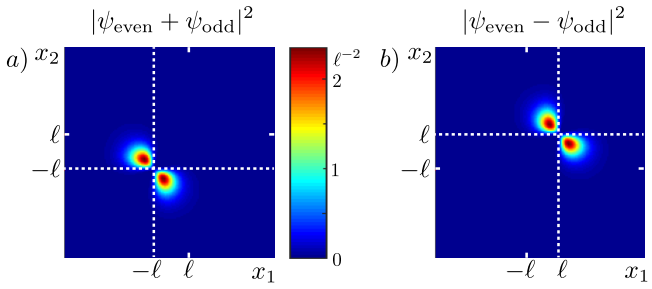

FIG. 8. (Color online) The modulus-square of the sum a) and of the difference b) of the wave functions of the two lowest two-particles eigenstates [even $\psi_{\rm even}(x_1, x_2)$ and odd $\psi_{\rm odd}(x_1, x_2)$] of the Hamiltonian (4) in the main text for $a_D = 6.3l$. The white dashed lines mark boundaries of the subwavelength domain, where the local dipole moment $d(x)$ changes its sign.

can be considered as q-independent, $\mathrm{Im}\,\epsilon^{(-)}_{n,q+k} \approx \mathrm{Im}\,\epsilon^{(-)}_{n}$. On the other hand, the q-dependence of $\mathrm{Re}\,\epsilon^{(-)}_{n,q}$ cannot be ignored, but the widths of $\mathrm{Re}\,\epsilon^{(-)}_{n,q}$ for the relevant bands are much smaller than the gap ($\approx \min|E_-(x)|$) between them and the dark state. As a result, the energy denominator in the expression for $\mathrm{Im}\,\delta\epsilon_{1,q-\mathrm{reg}}$ can be considered as q-independent, and $\mathrm{Im}\,\delta\epsilon_{1,q-\mathrm{res}}$, therefore, has the same form as $\mathrm{Im}\,\delta\epsilon_{1,q+\mathrm{reg}}$ with a different function $\gamma_1^{(0\to-)}(\epsilon, \Omega_p/E_R, \Delta/\Omega_p, \Gamma/\Omega_p)$. The sum of the two regular contributions from the + and − channels give the function γ_1 mentioned in the main text, Eq. (3). Similar considerations for the higher Bloch bands in the dark-state channel give that the dominant q-dependence of the decay rate originates from the antisymmetric part of the Bloch wave function (B11), and we obtain $\gamma_{n,q} = \gamma_n \cos^2(\pi q/2k - \pi n/2)$. In Figs. 7a and 7b we show the numerical results for the dependence of the functions γ_1 and γ_2 on the parameters of the system, both for the resonant and the off-resonant cases. We find out that the functions γ_n depend almost linearly on the parameter $\Gamma E_R^2/\Omega_p^2\epsilon$.

In calculating the resonant contribution $\delta\epsilon_{1,q-\mathrm{res}} = \delta\epsilon_{1,q\mathrm{res}}$, we can take into account the semiclassical character of the band n_0 and write $\epsilon_{1,q} - \mathrm{Re}\,\epsilon^{(-)}_{n_0,q+k} \approx v(q-q_*)$ for q close to q_* (see Fig. 2e in the main text). Here v is the group velocity (slope of the band n_0) at $q = q_*$. Keeping in mind that $M_{-n_0}(q)$ and $\mathrm{Im}\,\epsilon^{(-)}_{n_0,q}$ are slow functions of q, we can write the resonant contribution in the form

$$\delta\epsilon_{1,q\mathrm{res}} = |M_{-n_0}(q_*)|^2 \frac{1}{v(q-q_*) + i\Gamma_*/2},$$

where $\Gamma_* = -2\mathrm{Im}\,\epsilon^{(-)}_{n_0,q_*+k}$. The imaginary part of this expression has the typical resonant Lorentzian structure with the width proportional to Γ_*, and the height scales with Γ_*^{-1}. This structure is, therefore, visible if Γ_* is much smaller than the bandwidth $B_{n_0} \sim vk$ of the band n_0 (Fig. 2e in the main text). Another condition is related to the strength of the coupling $M_{-n_0}(q_*)$. This matrix element is visible only for zero and negative detunings, and is exponentially small for positive detuning when the wave function of the bright state in the band n_0 strongly oscillates in the coupling regions. The resonant contribution is therefore invisible in the latter case. For the resonant case with $\Gamma_* = \Gamma/4$ and $B_{n_0} \sim \sqrt{\Omega_c E_R}$, the visibility condition reads $\Gamma/\Omega_p \ll \sqrt{\epsilon\kappa}$, while for the negatively-detuned off-resonant case with $\Gamma_* \approx (\Omega_p/2\Delta)^2\Gamma$ and $B_{n_0} \sim \Omega_c\sqrt{E_R/|\Delta|}$, the resonances appear if $\Gamma/|\Delta| \ll \sqrt{\kappa}$.

To conclude, the discussion of the decay of the dark-state Bloch bands, we compare our results with those of the Kronig-Penney model for the periodic set of δ-functional potentials $\widetilde{V}_\delta(x) = (\hbar^2 A/2m)\delta(x)$ which strength has a small (negative) imaginary part, $A = \pi k/2\epsilon - iB$ with $0 < B \ll \pi k/2\epsilon$, mimicking the decay due to the coupling to other channels. The simplest way to obtain the energy spectrum in this case is by using the analytic continuation to the complex interaction strength in Eq. (B7) with the result for the decay rate in the lowest band

$$\gamma^{(\delta)}_{1,q} = -\frac{2}{\hbar}\mathrm{Im}\,\epsilon^{(\delta)}_{1,q} \approx \frac{E_R}{\hbar}\frac{32\epsilon^2 B}{\pi^3 k}\left(1 + \cos\left(\frac{\pi q}{k}\right)\right) \sim \cos^2\frac{\pi q}{2k},$$

which, in contrast to the expression (3) from the main text, is maximal in the center of the Brillouin zone.

Appendix F: Domain wall molecules - details of numerical analysis

The wave functions and the eigenenergies for the domain-wall molecules shown in Fig. 3 of the main text, are obtained by the numerical diagonalization of the two-particle Hamiltonian (4) of the main text with $V_L(x) = 0$. We performed our calculations for the case $d_1 = -d_2 = d$ such that the position-dependent dipolar moment of the dark state $d(x)$ crosses zero at $x = \pm\ell$ [$d(x) < 0$ for $|x| < \ell$], see Fig. 3a of the main text. In our calculations we limit the coordinates of the particles to the intervals $|x_{1,2}| \le 6\ell$ with zero boundary condition for the wave function. This region is then discretized into

a uniform grid of dimension 500×500. We also assume strong harmonic confinement for the motion in the transverse directions, such that the particles occupy only the lowest transverse Gaussian modes $\phi_0(\xi = y, z) = \exp(-\xi^2/2\ell_\perp^2)/\sqrt{2\pi^{1/2}\ell_\perp}$, with $\ell_\perp \ll \ell$. Under this condition, the effective interparticle interaction $V(x_1,x_2)$ is obtained by projecting the 3D dipole-dipole interaction onto the lowest transverse Gaussian modes,

$$
\begin{aligned}
V(x_1,x_2) &= d(x_1)d(x_2)\int_{\mathbb{R}^4} \frac{|\vec{r}_{12}|^2 - 3z_{12}^2}{|\vec{r}_{12}|^5} \prod_{i=1}^{2} \phi_0^2(y_i)\phi_0^2(z_i)\mathrm{d}y_i\mathrm{d}z_i, \\
&= d(x_1)d(x_2)\frac{F(x_{12}/\sqrt{2}\ell_\perp)}{2\sqrt{2}\ell_\perp^3} \\
&\to \frac{d(x_1)d(x_2)}{|x_{12}|^3}, \qquad |x_{12}| \gg \ell_\perp,
\end{aligned}
$$

where we assume dipoles oriented along the z-axis, $\vec{r}_{12} = \vec{r}_1 - \vec{r}_2$, and $F(s) = \sqrt{\pi}(2s^2+1)\exp(s^2)[1-\mathrm{erf}\,(s)] - 2s$ with $\mathrm{erf}\,(s)$ being the error function. We neglect here the contact term in the pseudopotential for the quasi-1D scattering with dipole-dipole interaction [3–5], as well as the short-range part of the interparticle interaction. The effect of these term is negligible because the wave function of the bound state becomes very small when two particles approach each other, see Fig. 8. This results from the strong repulsive interaction when the two particles are close on the same side of the interface. On the other hand, when they approach each other from different sides, the attractive interaction between them vanishes. This makes such configurations unfavorable for the bound state. Note that effective interaction $V(x_1,x_2)$ depends on $l_\perp$. This dependence, however, manifests itself only for $|x_{12}| \lesssim \ell_\perp \ll \ell$, and practically does not affect the results of our calculations (for $\ell_\perp \lesssim \ell/6$) because the wave functions for the states of interest are very small in this region (see Figs. 8a and b).

The lowest two eigenstates are found to be symmetric (even) and antisymmetric (odd) superpositions of the two states in which the molecular wave function is located around $x = -\ell$ or $x = \ell$ (dashed circles in Fig. 3a of the main text and Fig. 8), with the corresponding wave functions $\psi_{\mathrm{even}}(x_1, x_2)$ and $\psi_{\mathrm{odd}}(x_1, x_2)$. To demonstrate the structure of these states we plot the modulus squared of the sum (Fig. 8a) and of the difference (Fig. 8b) of their wave functions for the case $a_D = 6.3l$. The dependence of the eigenenergies of these states on the strength of the interparticle interaction is presented in Fig. 3a of the main text. The energy difference ΔE between the two eigenstates provides the molecular hopping element, $J_{\mathrm{pair}} = \Delta E/2$ (see Fig. 3c of the main text), between the domain-wall molecular states at $x = -\ell$ (Fig. 8a) and $x = \ell$ (Fig. 8a).

We also performed the analogous calculations for the case of three particles and found the formation (for $a_d \gtrsim 5\ell$) of the three-body bound state (trimer) in which one particle is in the region $|x| < \ell$ and the other two

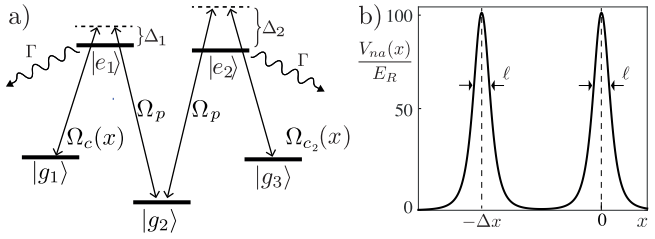

FIG. 9. Panel a) Double-Λ configuration with two position-dependent Rabi frequencies of the control fields $\Omega_{c_1}(x)$, $\Omega_{c_2}(x)$ and two homogeneous Rabi frequencies Ω_{p_1}, Ω_{p_2} of the probe fields (see text). b) Dark-state non-adiabatic potential $V_{na}(x)$in units of the recoil energy E_R for the case $\Omega_{c_1} = \Omega_{c_2}$, $\Omega_{p_1} = \Omega_{p_2}$, and $\epsilon_1 = \epsilon_2 = 0.1$.

are on the opposite sides of this region. The formation of the trimer can be intuitively understood by considering the interaction of the two particles forming a domain molecule, say at the interface $x = -\ell$, with the third particle in the region $x > \ell$. It is easy to see that this interaction is attractive, thus giving rise to the formation of the bound state. This also explains why the threshold for the formation of the trimer is slightly lower than that ($a_d/\ell \geq 6$) for the dimer (molecule).

Appendix G: Double-peaked subwavelength optical barriers

We present here another example for a laser-atom configuration as an atomic double-Λ configuration, which leads to the double-peaked structure in the non-adiabatic potential of the dark state. This is similar to that presented in Fig. 4 of the main text, but with the possibility of controlling the spatial separation between the peaks. In contrast to the atomic scheme described in the main text, we consider here three ground states $|g_1\rangle$, $|g_2\rangle$, and $|g_3\rangle$, and two excited states $|e_1\rangle$ and $|e_2\rangle$, which might belong to Zeeman manifolds with different angular momentum J and, therefore, the laser couplings between them are generated by two independent control and two independent probe lasers. The lasers are tuned to satisfy the Raman on-resonance condition between the ground states $|g_1\rangle$ and $|g_2\rangle$, as well as between $|g_2\rangle$ and $|g_3\rangle$, with the constant Rabi frequencies Ω_{p_1} and $\Omega_{p_2}$for the probe beams, and position dependent Rabi frequencies $\Omega_{c_1}(x) = \Omega_{c_1}\sin(kx)$ and $\Omega_{c_2}(x) = \Omega_{c_2}\sin[k(x+\Delta x)]$ (with off-set Δx) for the control beams (see Fig. 9a). For a weak probe beams, $\epsilon_i = \Omega_{p_i}/\Omega_{c_i} \ll 1$, the calculated non-adiabatic potential for the dark state $|E_0\rangle \sim \Omega_{p_1}\Omega_{c_2}(x)\,|g_1\rangle - \Omega_{c_1}(x)\Omega_{c_2}(x)\,|g_2\rangle + \Omega_{p_2}\Omega_{c_1}(x)\,|g_3\rangle$ contains two peaks of widths $\ell_i \sim \epsilon_i\lambda/2\pi = \epsilon_i/k$: the first one originates from the left leg of the double-Λ system, and a second one from the right leg. These are separated by the distance Δx (we assume $\Delta x > \ell_i$). The separation of the two barriers can, therefore, be controlled by tuning the relative phase $k\Delta x$ between the control

beams. Fig. 9b shows the resulting non-adiabatic potential $V_{na}(x)$ in units of the recoil energy $E_R = \hbar^2 k^2/2m$ for the case $\Omega_{p_1} = \Omega_{p_2}$ and $\epsilon_1 = \epsilon_2 = 0.1$.

Appendix H: Measurement proposals

Here we briefly discuss possible measurement schemes for testing the results of the paper related to both single-atom physics and two-atom/many-atom physics.

On the level of single-atom physics (i.e. both for the 1D bandstructure and, in a similar way, for the double wire/layer) time of flight would be a natural way to map the spatial structure to momentum structures [2, 6, 7]. The new aspect here is the correlation (as given by the spatial variation of the dark state) between the atomic internal states and subwavelength structures.

Another possibility would be to reverse in time our loading protocole (see Section D), so that subwavelength structures are mapped to band fillings etc. in standard optical lattices, where well-developed tools exist for read out [7]. Finally, one can modulate the 'dark state' lattice parameters, and perform a spectroscopy by driving transitions between bands (see for example[2, 8, 9]). On the level of two and three atoms, the same strategy results in the mapping of the two- and three-body bound states to occupations of atomic vibrational levels in the lattice $V_L(x)$. Another way to perform spectroscopy of the bound pairs and trimers would be driving with an external field (e.g. RF [10, 11]) which couples to the atomic internal states (analog to the coupling to spin-degree of freedom in the case of atomic Cooper pairs [12, 13] and Feshbach molecules [14]), or to use a lattice modulation spectroscopy.

We plan to include the details of all the topics discussed in the Supplemental Materials in Ref. [15].

[1] E. Merzbacher, *Quantum Mechanics* (Wiley, 1998).
[2] I. Bloch, J. Dalibard, and W. Zwerger, Rev. Mod. Phys. **80**, 885 (2008).
[3] S. Yi and L. You, Phys. Rev. A **61**, 041604 (2000).
[4] S. Ronen, D. C. E. Bortolotti, D. Blume, and J. L. Bohn, Phys. Rev. A **74**, 033611 (2006).
[5] S. Sinha and L. Santos, Phys. Rev. Lett. **99**, 140406 (2007).
[6] F. Gerbier, A. Widera, S. Fölling, O. Mandel, T. Gericke, and I. Bloch, Phys. Rev. A **72**, 053606 (2005).
[7] I. Bloch, Nature Physics **1**, 23 (2005).
[8] T. Stöferle, H. Moritz, C. Schori, M. Köhl, and T. Esslinger, Phys. Rev. Lett. **92**, 130403 (2004).
[9] C. Kollath, A. Iucci, T. Giamarchi, W. Hofstetter, and U. Schollwöck, Phys. Rev. Lett. **97**, 050402 (2006).
[10] S. Gupta, Z. Hadzibabic, M. Zwierlein, C. Stan, K. Dieckmann, C. Schunck, E. Van Kempen, B. Verhaar, and W. Ketterle, Science **300**, 1723 (2003).
[11] Y. Shin, C. H. Schunck, A. Schirotzek, and W. Ketterle, Phys. Rev. Lett. **99**, 090403 (2007).
[12] P. Törmä and P. Zoller, Phys. Rev. Lett. **85**, 487 (2000).
[13] C. Chin, M. Bartenstein, A. Altmeyer, S. Riedl, S. Jochim, J. H. Denschlag, and R. Grimm, Science **305**, 1128 (2004).
[14] C. A. Regal, C. Ticknor, J. L. Bohn, and D. S. Jin, Nature **424**, 47 (2003).
[15] M. Łącki, A. Elben, H. Pichler, M. Baranov, and P. Zoller, in preparation.